Eng Int Syst (2022) 5: 377–385

Engineering
Intelligent Systems

Multi-Feature Fusion Algorithm Based on AR-Based Panoramic Image Processing Technology Inside a Wind Turbine

Jin Xu[1,2,a,*], Jianing Zhang[3,b], Long Ban[3,c] and Guangbo Feng[3,d]

[1] *China lvfa Investment Group Co., Ltd, Beijing, 100020, PRC*
[2] *Ducheng Weiye Group Co., Ltd, Beijing, 100032, PRC*
[3] *Xuchang Xuji Wind Power Technology Co., Ltd, Xuchang, 461199, PRC*

Image fusion is not only a simple image synthesis and superposition process, it is also an organic combination of the advantages of the information contained in each image data. It can also improve the clarity and understanding of the image, achieve further image segmentation, target detection and recognition, and provide a better understanding of image processing and more effective information. This article introduces the multi-feature fusion algorithm based on AR-based panoramic image processing technology of the fan. This paper adopts a matching algorithm based on additional landmarks through the calibration of the vision system, completes the positioning of the landmarks in the space, so that the positioning of the landmarks can be tracked in real time in the process, and through the augmented reality image fusion method, a virtual 3D model is created using 3D software, positioning the fiducial point of the real world to be enhanced, and then fusing the real scene image and the virtual image graphics according to a certain relative position space. The experiment results show that the execution efficiency of the multi-feature fusion algorithm is 1.23 times better than the SIFT algorithm and its matching accuracy is 19.85% higher than that of the SIFT algorithm. This table reflects the performance of the multi-feature fusion algorithm for larger viewing angle transformation and contrast. The object image has strong robustness and matching performance in complex situations.

Keywords: AR Technology; Fan Internal Structure; Panoramic Image Processing Technology; Multi-Feature Fusion Algorithm; Matching Algorithm

1. INTRODUCTION

With the rapid development of science and technology, processing digital images has become increasingly complex. Due to the limitations of the physical characteristics of the image sensor, the imaging mechanism, the observation angle, and the imaging conditions, a single image sensor usually cannot extract enough information from the scene, and is unable to receive clear, information-rich, and accurate scene images. Image fusion technology, an important method to solve this problem, has attracted much attention. Regarding the dynamic target monitoring and feature matching of sequence images, a large body of research has been conducted across the globe and significant progress has been made. However, the research content mainly focuses on the splicing and fusion of plane images. The method of plane image and fusion component can be used as a reference for 3D stitching and fusion. Stitching and fusion cannot directly use 3D images of different proportions. In addition, the method is very different.

Although the panoramic image stitching and fusion method has a certain reference effect on three-dimensional stereo stitching and fusion, it cannot be directly used for the stitching

*Corresponding author [a]Email: pingpangzhiwang@163.com [b]Email: hankrui201912@126.com [c]Email: banlong8124@163.com [d]Email: 15222693020@163.com

and fusion of stereo images of different scales. The technology and methods are also very different. In multi-scale, it can accurately monitor and match the target. Dynamically, the stitched stereo image and its feature matching and fusion in the reconstruction of the 3D image from the 2D image sequence of different scales needs further research. The three-dimensional reconstruction of monocular image sequences based on image stitching and fusion technology can be used for accurate target tracking, and can also be used for target reconstruction in aerial image sequences. Therefore, this research has important practical significance and has important potential application prospects in aviation, military and politics.

Shim [1] proposed a novel method to automatically adjust camera exposure for image processing and computer vision applications on mobile robot platforms. Because most image processing algorithms rely heavily on low-level image features based mainly on local gradient information, Shim found that the amount of gradient can determine the appropriate exposure level so the camera can capture important image features in a manner that is stable in relation to lighting conditions. However, due to the influence of many external factors in image exposure, the accuracy of the results is reduced [1]. Guan [2] considered the deficiencies of basic LBP features in face detection and used unified MB-LBP features and unified rotation invariant LBP features to describe the local texture features of the face. The edge orientation field feature based on the Canny operator is combined with the aforementioned two features to describe face information. Finally, the Gentle Adaboost classifier is designed to classify all the extracted features. However, due to the few types of Haar-like rectangular features, this will result in the classifier training time being too long [2]. Wu [3] proposed a novel point matching algorithm. An improved random sample consensus (RANSAC) algorithm called Fast Sample Consensus (FSC) is proposed. It divides the data set in RANSAC into two parts: the sample set and the consensus set. The sample set has a high correct rate, while the consensus set has a large number of correct matches. Wu verified the performance of the proposed method by evaluating these measures and mosaic images. But compared with RANSAC, FSC obtains more false matches in more iterations [3].

The innovation of this article is to introduce the theory of scale feature transformation, extract the feature points of the image by writing the program code and analyzing it, and then introduce the development ideas of the region, use the output feature as the seed point, let it follow its. own The set development standard is developed to obtain the clear area in the image, and finally the replacement image is used to achieve the final image fusion through the proposed fusion rule.

2. MULTI-FEATURE IMAGE FUSION ALGORITHM

2.1 Image Fusion Algorithm

(1) Based on image grayscale

The fusion algorithm based on grayscale images is simple and easy to operate. The method proposed in this paper is the weighted average method based on grayscale images [4].

1) Selection method: Convert the collected image into a grayscale image and use a table to record the pixel value of each point. The pixel value of each point in the repeated area defines the limit value. If the pixel value difference of the two points is within the limit value selection range, only the pixel value of the change point in the image is selected as the pixel value of the point after the grid. This fusion method is simple and easy to implement, but the transition of the accessory area is not smooth, and the gap of the accessory is more likely to be affected by the appearance [5].
2) Weighted average method: Each pixel value in the overlapping area of the two images must be weighted according to the distance from the edge of the overlapping area. The closer to the edge, the smaller the weight coefficient [6]. The weighted pixel value is calculated based on the weighted coefficient, and the weighted average pixel value corresponds to the position image of the pixel in the frame. The weighted average can be a linear weighting or a weighting coefficient in the form of a trigonometric function, which can calculate a more realistic and effective weighting result.
3) Optimization method: According to the needs of different types of grids and image fusion, the optimization method is a hybrid gray-scale fusion algorithm, or a variety of fusion methods are used to improve the image fusion effect according to the characteristics of the image vascular coating area.

Image processing must be performed in a specific color space model and different models will obtain different image processing effects. Common color space models are composed of YUV, HSI, etc. [7].

(2) Based on YUV

In the YUV color model, AAA represents light intensity, and BBB and CCC represent color and saturation respectively. Compared with the RGB space model, the YUV model is more suitable for the visual habits of the human eye. It can separate the intensity of light, thereby reducing the influence of light and reflection on color recognition [8]. Another advantage is that there is a linear conversion relationship between it and the RGB space model. Formula (1) is the relationship between linear conversion. Through calculation, the conversion between models can be completed quickly. Some researchers choose the YUV color space model as the basis for target recognition [9–10].

$$\begin{bmatrix} Y \\ U \\ V \end{bmatrix} = \begin{bmatrix} 0.23 & 0.60 & 0.11 \\ -0.15 & -0.30 & 0.11 \\ 0.62 & -0.52 & -0.1 \end{bmatrix} \begin{bmatrix} R \\ G \\ B \end{bmatrix} \quad (1)$$

The HSI space model is a unified spatial color model based on the principles of vision, which is in line with human visual perception where H represents color, that

is, the color of light related to the wavelength of the main light wave in the mixed spectrum and the light waves of different wavelengths appear differently; S represents the saturation of the color, that is, the depth of the color where the saturation is proportional to the degree of color, the higher the degree of color, and vice versa; and I represents brightness, which usually refers to the degree of brightness that the human eye can perceive [11].

The H element of the HSI space model can reflect the accuracy of the color type and reduce the sensitivity to external light changes. The three components of the space model are not related to each other, and correspond to the characteristics of colors perceived by the human eye. These three components are suitable for expressing the differences between different colors [12]. For items with the same color features, the H conversion range is relatively stable. S can be used as the main color feature or as an auxiliary criterion to enhance the effect of image recording. I is usually not used as a criterion. There is a nonlinear conversion from the RGB color space model to the HIS color space model, as shown in formula (2) (3) (4):

$$H = \cos^{-1}\left\{\frac{\frac{1}{2}(R-G)+(R-B)}{\sqrt{(R-G)^2+(R-B)(G-B)}}\right\} \quad (2)$$

$$S = 1 - \frac{\min(R,G,B)}{I} \quad (3)$$

$$I = \frac{(R+G+B)}{3} \quad (4)$$

The fusion algorithm based on color space conversion converts the RGB color space model of the image into other color space models such as the HSI model. Then, the parameters with larger differences in the transformed spatial model are selected as the fusion variables of the image fusion [13]. Finally, the fusion image is restored to the RGB color space model to realize the capture of the fusion image.

2.2 Image Matching Algorithm With Additional Identification Points

When processing images, in order to extract several feature points with precise coordinates, it is usually necessary that the surface of the measured object has rich texture information which is easy to identify and output, so that the image taken after the measured object is taken. Obvious grayscale changes can be used to match images [14]. However, in digital industrial photography, because its machinable surface usually lacks sufficient physical texture to support matching or it is difficult to identify and export physical textiles and their characteristics, digital industrial photography has low precision and is therefore unsuitable for high-precision industrial photography. Therefore, it is usually necessary to use artificial marker points as the feature points of the target to be measured to assist the measurement [15].

Digital industrial photography based on artificial markers

Since the received image is an isolated mark, dot or dot, when used as a matching primitive for matching images, the gray information of additional pixels around the pixel can be used, while the straight line or auxiliary matching of surface features is impossible to match. Therefore, the traditional image matching algorithm based on grayscale and features is no longer suitable for this. In high-precision digital industrial photography, it is necessary to design a new image matching algorithm based on the characteristics of artificial markers and their images [16]. At present, there are very few investigations on digital industrial photography algorithms in China. There are two main algorithms:

(1) Image point matching method based on drive file

The drive record used for correction is the approximate value of the three-dimensional coordinates of the target area of the target point to be measured. It must be obtained in advance from other measurement systems and combined with the drive position file to complete the matching process [17]. When the deformation of the measured object is small, this method works well, but it cannot handle a large deformation of the measured object. Due to the limitations of the driving record, it cannot meet the needs of digital industrial dual-camera photography for the real-time processing of photographic data [18].

(2) Image point matching method based on nuclear surface grouping

This algorithm restrains the influence of the angle between the photograph and the nuclear horizontal plane on the projection conversion to a plane limit, and the restriction conditions are better. But because the algorithm needs to group three images, additional constraints on the third image are needed to improve the accuracy of matching. Therefore, it cannot be directly used to match digital industrial dual-camera images [19].

2.3 Multi-Feature Fusion Algorithm

As a local feature matching algorithm, scale-invariant feature transform (SIFT) has a good rotation conversion ability and good patience, but it is more sensitive to visual changes [20]. R-SILBP is very resistant to changes in light, contrast and angle. Both SIFT and RILBP algorithms have the advantage of scalability. The matrix of these two characteristics described in this article is linear.

SIFT is used to extract the imaging medium, establish the DoG scale space of i images, and use the Gaussian kernel function to blur the image to obtain the DoG pyramid. The Gaussian kernel function appears in equation (5):

$$D(x,y,r) = \frac{1}{2\pi r^2} e^{\left(-\frac{(x-u/2)^2+(y-v/2)^2}{2r^2}\right)} \quad (5)$$

In expression (5), u and v represent size corresponding to Gaussian standards. To obtain better stability and uniqueness, a DoG control gate is used to make DoG extreme points in image space and proportional space, and compare each pixel with 24 nearby points. When the value of all adjacent points

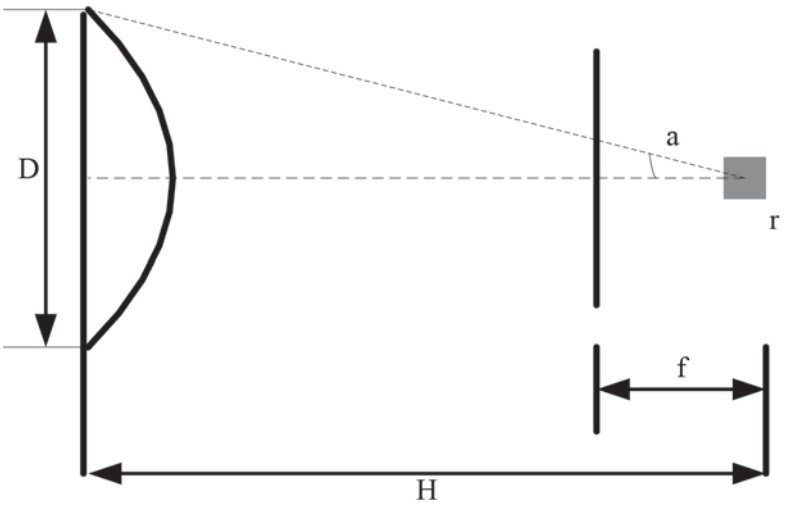

Figure 1 Panoramic mirror size design.

$$u(x, y) = \sqrt{(N(x+1, y) - N(x-1, y))^2 + (N(x, y+1) - N(x, y-1))^2} \tag{6}$$

$$\omega(x, y) = \tan^{-1} \frac{N(x, y+1) - N(x, y-1)}{N(x+1, y) - N(x-1, y)} \tag{7}$$

is exceeded (or below), it is set as an extreme point. The Hes-sian matrix of 3×3 is used to eliminate unstable feature points [21].

Then, values are assigned to the feature point directions. The modulus of the gradient $u(x, y)$ and $\omega(x, y)$ directions are shown in equations (6) and (7) respectively:

Perform R ILBP feature vector generation for each point on the feature point set extracted by SIFT, as follows:

First, in the $(2n-1) \times (2n-1)$ pixel area centered on Q, find the R ILBP feature centered on each pixel Q, expressed as:

$$lbQ(j = 1, 2, \ldots, (2n+1)^2) \tag{8}$$

Second, calculate the weighting coefficient, that is, the contribution value of P to using formula (9):

$$w_j = \frac{1}{2\pi\sigma_0^2} e^{-\frac{(b_j, c_j)^2 + (b_i, c_i)^2}{2\pi\sigma_0^2}} \tag{9}$$

where (b_j, c_j) and (b_i, c_i) are the coordinates of the pixel point and the center point in the original pixel area, and σ_0 is the selected constant.

3. AR'S FAN PANORAMIC IMAGE FUSION EXPERIMENT

3.1 Panoramic Vision System Design

The hyperboloid mirror is used for framing. While the perspective imaging lens of the camera faces the hyperboloid mirror, the focus of the hyperboloid mirror is exactly the same as the optical center of the camera. According to the one-point camera principle, a one-point refraction panorama can be formed. The imaging system shows the geometric relationship between the camera and the mirror, as illustrated in Figure 1. The design of the mirror depends on the decision of other parameters of the system, so the most important thing in the design of the panoramic image system is the design of the excessive mirror. When the design of the external rearview mirror is completed, the overall design of the corresponding visual function and visual display is also completed. In recent years, with the continuous development of panoramic imaging technology, the design method of the mirror is constantly updated. This document uses the most ideal design method proven in practical applications and designs the parameters of the mirror [22].

The idea of designing the mirror in this document is to first determine the position of the rearview mirror and the maximum angle of view, then the camera is adjusted to determine the maximum size of the mirror and finally to determine the size of the mirror. The details are as follows.

Choose r as the short side size of the camera imaging unit. The focal length of the lens is expressed by f, and these two indexes are fixed parameters [23]. Take the distance between the rear surface of the mirror and the perspective center of the camera lens as H, and the diameter of the top of the mirror as R.

3.2 Three-Dimensional Model of the Fan

This experiment uses the model-making method, that is, according to the actual model of the impeller and related parameters, the periodic characteristics of the CT magnetic flux flying piece structure are considered in the modeling process, and the turbine unit in Gambit is used to determine the flow field model of a single blade. This method is more

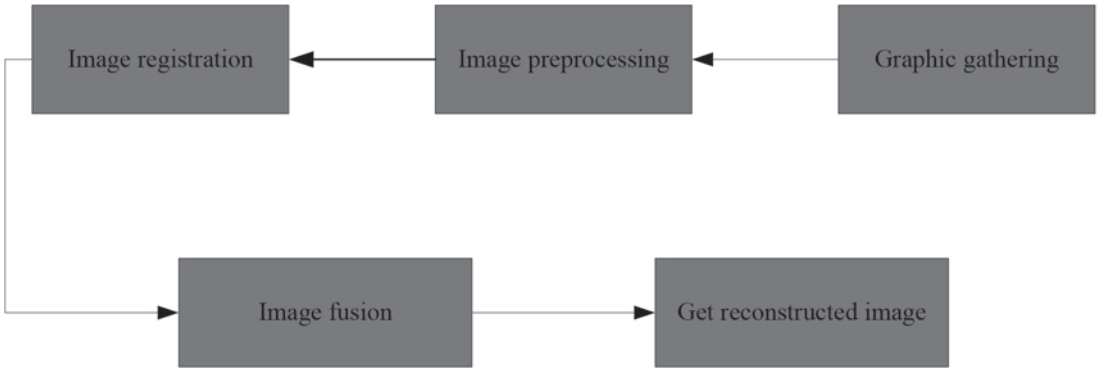

Figure 2 Flow chart of image stitching and fusion.

convenient and effective than general modeling methods [24]. When creating a model using turbine elements, the steps for points, lines, surfaces, and volumes should be followed. The most critical step is to compile a file with .Tur. In this file, we need to define the relevant parameters of the component blade [25].

Refer to the relevant parameters of the existing fan, use the Cartesian coordinate system to set the rotation axis of the leaflet as the X axis, specify the position of the hub and the surface of the housing as the coordinate form, use the plan view software to select 7 components from the center of the housing, and receive the different coordinate points of each interface which are put into the file in the form of pressure surface and attraction surface. In the area, please note that the reported coordinate sequence is from the positive pressure surface to the negative pressure surface, and then from the front end to the back end of the blade. After compiling the file, for the next calculation, input it into Gambit [26].

After inputting the file in Gambit, we can get a schematic diagram of the shape of the leaf. The turbine unit is then used to determine the inlet and outlet of the air flow associated with the pool, the casing and each part, and then this is each relevant surface of the blade. This step is also equivalent to defining the boundary conditions of the blade. After completing the relevant definition settings, a model of a single blade will be created, and the last step is to divide the mesh. Through division, an unstructured grid of about 140,000 squares is obtained. After checking, the network slope is less than 0.78, which meets the calculation requirements [27].

3.3 AR 3D Tracking Standard Experiment

The method reported in this document is tested in the form system. The CPU uses a dual-core Intel core i3 processor and a 2.76GHz frequency clock, and the graphics card uses a GeForce GTS 420. The input device is a Logitech HD C360 camera, the input video resolution is 480 × 640, the frame rate is between 25–35fps, and the output device is an ordinary liquid crystal display [28].

The experiment gives an example of real-time 3D monitoring and recording on the internal office platform: a reconstructed cloud of 3D points in the scene, a total of 7564 points in 3D, and the preprocessing sequence contains 78 frames of images. At the bottom is the selected 16 basic frame images which basically cover the entire scene, the amount of 3D data between them is small, including most 3D feature points.

To verify the real-time nature of the recording method, experiments were conducted while executing its unit. In the experiment, SiftGPU was used to export SIFT features. Since each unit runs independently, as long as the computing power is sufficient, the frame rate of this method is determined by the most time-consuming unit [29]. The SIFT point output unit lasts for 44ms, so the frame rate is about 19fps. The delay of this method is the sum of the execution time of each unit, which is about 78ms. In fact, because the key frames are independent of each other, if the key frames of the image input perform feature matching in parallel, the effect of parameter 61547 on the delay can be ignored, so the delay will be further shortened. In practical applications, users will not realize that the delay is within 100 milliseconds, so this article will improve the cloud point-based writing method to meet the basic real-time requirements.

3.4 Multi-Feature Image Fusion Experiment

Image combination and fusion technology is developing rapidly. Through the combination and fusion of multiple images, a more accurate, comprehensive and reliable image description of the same scene can be obtained, which has become one of the hot spots of computer vision. Image fusion consists of the following steps, as shown in Figure 2:

Image acquisition involves shooting the target scene from multiple angles. In the subsequent image stitching, the two images will maintain a 20% overlap area. Image preprocessing involves changing the location of the collected images, suppressing or reducing the noise points, and connecting the collected high-quality source images. First, the error rate is reduced in the image matching stage. The alignment of the image involves comparing the features of the image to find similar features in two adjacent images, determine the overlapping area, and prepare to merge these areas. The image fusion uses similar features of the image to perform average weighting. To eliminate the fusion gap, the synthesized image is smoothly transferred to the synthesized area. Through these steps, the reconstructed image after stitching can be obtained [30].

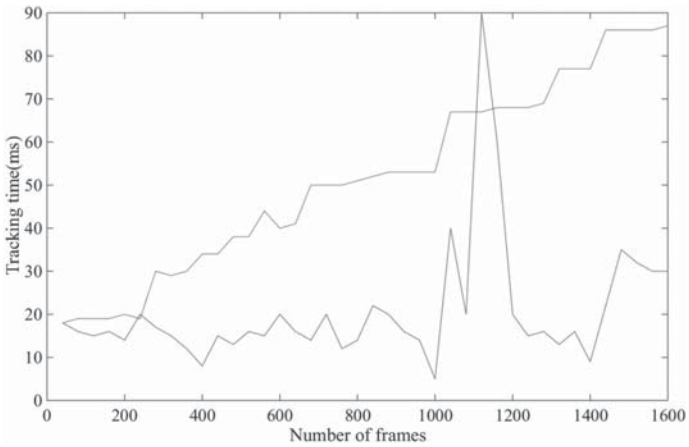

Figure 3 The relationship between the scale of the dot graph and the tracking time.

Table 1 Time-consuming distribution of cluster adjustment under different scales.

Number of key frames	1–39	40–79	80–139
Local cluster adjustment	160ms	255ms	435ms
Global cluster adjustment	388ms	1.6s	6.7s

4. MULTI-FEATURE IMAGE FUSION ANALYSIS

4.1 Analysis of AR Registration and Tracking Technology

Figure 3 plots the changes of the tracking time and the scale of the point map as the number of frames increases. It can be seen from the figure that as the dot map grows, most of the image frame tracking can be completed in about 20 ms, but the tracking is lost at about 1320 frames. At this time, the relevant frames are performed through the recovery program. Repositioning takes about 90 ms per frame; at about 1530 frames, because the camera moves far away from the desktop, a large number of feature points appear, and the tracking process takes about 30 ms per frame. Experiments show that the method discussed in this paper can track the image sequence in real time.

The time required to perform a certain step in the rendering process is difficult to determine because this varies under different image scales and scene structures. Nevertheless, we can still describe the approximate time-consuming distribution of cluster adjustment. The experiment results are shown in Table 1. The table shows an average time-consuming amount. the average time required. It can be seen that the method proposed in this paper can be used when the number of key frames is less than 100. Meet the real-time requirements. When there are more than 100 frames, the proposed method will not be able to keep up with the movement of the camera and will often result in failure. It can only converge when the camera remains still or the camera returns to a drawn area. When there are more than 150 frames, even the local cluster adjustment is It will take a few seconds. In contrast, global bundling adjustment will take longer for different key frame numbers. When it exceeds 50 frames, it can no longer meet the real-time requirements.

It can be seen that the method proposed in this paper separates tracking and drawing through parallel threads and replaces the global clustering adjustment strategy with a local part, which improves the real-time performance of tracking to a certain extent, and at the same time, it can handle larger-scale scenes.

4.2 Analysis of Identification Point Matching Algorithm

From the experiment results, it can be seen that after the improved matching algorithm processes the matching point set, the mismatched points are eliminated. Therefore, the proportion of outliers corrected by the matching algorithm is reduced to 0. As the proportion of outliers increases, the number of sampling increases, resulting in an increase in the calculation time and the relationship is generally linear, but the calculation accuracy of the corrected matching algorithm does not decrease, and the wrong matching points can still be accurately eliminated. To verify the superiority of the algorithm and the improvement of the matching algorithm, the calculation efficiency and accuracy of the traditional matching algorithm under the same conditions and the improved matching algorithm in this paper are compared. The statistical results are shown in Figure 4:

An analysis of the experiment results shown in Fig. 4 enables the following conclusions to be drawn:

(1) The improved matching algorithm proposed in this paper eliminates mismatched points. As the proportion of out-of-sample points increases, the algorithm in this paper always maintains high calculation accuracy, accurately eliminates mismatched points, and ensures that the outliers of the matching point set after the algorithm runs. The ratio is 0, which is mainly due to the improvement of the new error weighting function in the selection of

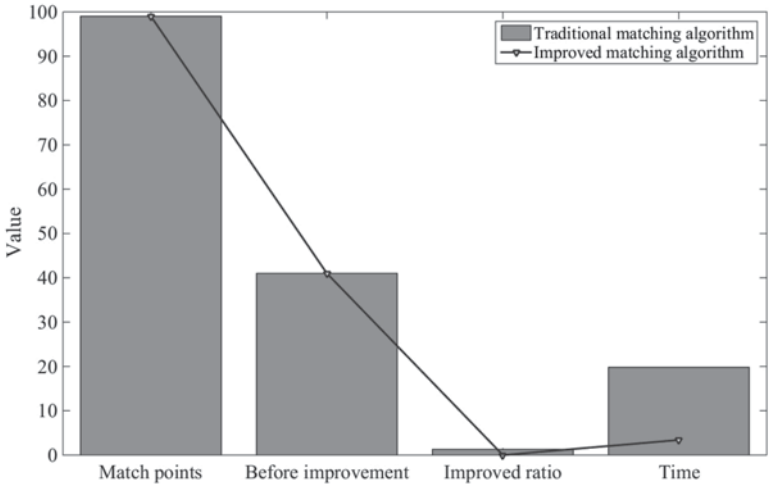

Figure 4 Comparison of different algorithms.

Table 2 Comparison of recall rates of different algorithms.

Algorithm	Rotation transformation	Contrast	Scale scaling	Mixed situation
SIFT	94	96	93	65
Sift+VFC	98	99	94	72
Multi-feature fusion	97	99	93	85

interior points and the improvement of the sampling process by the random block matching point selection method. The calculation time increases with the increase of the ratio of the exterior points, which is roughly a linear relationship. This is mainly related to the change in the sampling frequency with the proportion of outliers.

(2) Compared with the traditional matching algorithm, the improved matching algorithm proposed in this paper has higher calculation accuracy under the same circumstances. When the traditional matching algorithm cannot accurately eliminate the wrong matching points, the improved matching algorithm can still eliminate all errors. The matching point and the calculation time is much shorter than that of the traditional matching algorithm and the calculation efficiency is greatly improved. This is mainly due to the following aspects: the reduction of the minimum sample set, the reduction of sampling times and the optimization of the algorithm in the pre-inspection process.

4.3 Multi-Feature Fusion Algorithm Analysis

To avoid the problem of a large numerical deviation caused by the small number of matching points, in the case of viewing angle change and large contrast, this paper uses two sets of different feature points to demonstrate the efficiency and accuracy of the algorithm and the original SIFT. The statistical comparison of degree is shown in Table 2.

The number of feature points extracted for the first time refers to the number of feature points extracted from the target image; the number of points after matching refers to the number of matching points obtained after the target image and the image to be matched are matched using the corresponding matching algorithm; the matching conditions are all the original image and the larger view angle transformation, Contrast transformation and rotation transformation of the image to be matched, the matching algorithm corresponding to the algorithm in this paper is a high-dimensional data scalable nearest neighbor algorithm combined with VFC, and the matching algorithm corresponding to the SIFT algorithm is a fast nearest neighbor algorithm. Mismatch points refer to the number of mismatch points that appear on the matching result graph. The matching accuracy is the quotient obtained by dividing the correct matching pair by the number of matching points. The results are shown in Figure 5:

The experiment results show that in the case of rotation transformation, the recall rate of this algorithm is 2.89% higher than that of the SIFT algorithm. In contrast, the recall value of this algorithm is 3.89% higher than that of SIFT, which indicates that the algorithm proposed in this paper has a larger rotation angle and contrast transformation and it has stronger resistance than SIFT. In the case of scale transformation, the resistance of this algorithm is similar to that of SIFT. In the case of large visual transformation and contrast transformation, the accuracy of this algorithm is 19.85% higher than the original SIFT, which is higher than SIFT+vfc by 12.79%. For the same feature points and matching pairs, the recall rate of the proposed algorithm is 28% higher than that of the SIFT algorithm when the visual transformation and contrast transformation are large, indicating that the proposed algorithm is more effective for a larger viewing angle transformation and contrast. The object image has strong robustness and matching performance in complex situations. In terms of execution efficiency, the algorithm in this paper is 1.23 times more efficient than SIFT.

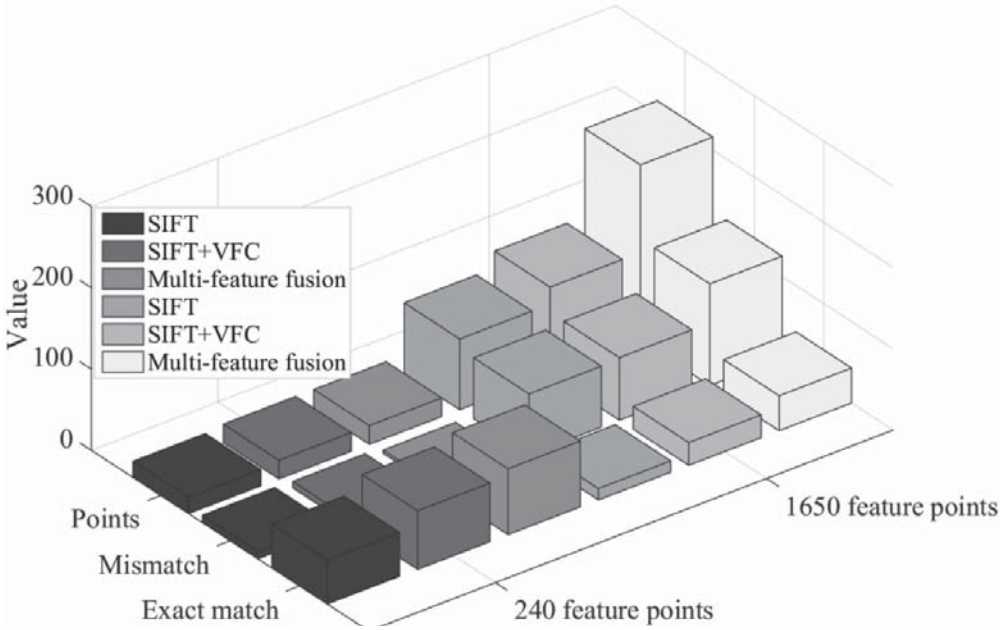

Figure 5 Results of different algorithms at different matching points.

5. CONCLUSIONS

This paper studies the registration method based on three-dimensional monitoring and reconstruction, and proposes a current-based parallel monitoring and planning method technology. Taking into account the current 3D monitoring and reconstruction methods, tracking and production are mutually restricted, which will affect real-time performance, and cannot automatically repair monitoring failures. The parallel monitoring and tracking method adopts the idea of parallel computing to separate monitoring and performance, monitor the movement of the camera, and design a point map to improve the real-time configuration of the configuration. The recovery strategy of the failure point is extended and the real-time adjustment of the failure point is extended. Robustness is improved through the establishment of monitoring quality assessment; the local cluster adaptation strategy is used to replace the global set adjustment, which improves the calculation efficiency and parameter resolution accuracy.

The dual-camera mapping algorithm based on the nonlinear relationship proposed in this paper can effectively achieve image matching and can meet the observation requirements of the dual-camera digital industrial photography system for dynamic data field processing. The improved matching algorithm can effectively eliminate and match point sets. Points that do not match are more effective against traditional matching algorithms.

This article takes the imaging characteristics of image fusion as the basis, randomly selects the feature points of a natural image and sets it as seed points, and develops and locates the clear scene. However, this article is not only trying to accurately locate the clear scene of the fused image. Rather, to conduct more in-depth research, this is also an area that needs to be further explored in the future. Human vision cannot judge the effect of image fusion. This is because the human eye is affected by many factors. Therefore, a more objective evaluation of the quality of image fusion is also a problem that needs further research.

REFERENCES

1. Shim I, Oh T H, Lee J Y, et al. Gradient-Based Camera Exposure Control for Outdoor Mobile Platforms. *IEEE Transactions on Circuits and Systems for Video Technology*, 2019, *29*(6):1569–1583.
2. Guan L, Tong Y, Li J, et al. An online surface water COD measurement method based on multi-source spectral feature-level fusion. *RSC Advances*, 2019, *9*(20):11296–11304.
3. Wu Y, Ma W, Gong M, et al. A Novel Point-Matching Algorithm Based on Fast Sample Consensus for Image Registration. *IEEE Geoence & Remote Sensing Letters*, 2017, *12*(1):43–47.
4. Lie D, Trivedi A R, Mukhopadhyay S. Impact of Heterogeneous Technology Integration on the Power, Performance, and Quality of a 3D Image Sensor. *IEEE Transactions on Multi-Scale Computing Systems*, 2017, *2*(1):61–67.
5. Asgari A R, Ghorbanian T, Dadashzadeh D, et al. Solid Waste Characterization and Management Practices in Rural Communities, Tehran and Alborz (Iran). *Journal of Solid Waste Technology and Management*, 2019, *45*(1):111–118.
6. Yamini K, Renganathan B, Ganesan A R, et al. Clad modified optical fiber gas sensors based on nanocrystalline nickel oxide embedded coatings. *Optical Fiber Technology*, 2017, *36*(jul.):139–143.
7. Mills A R, Kadirkamanathan V. Sensing for aerospace combustor health monitoring. *Aircraft Engineering and Aerospace Technology*, 2020, *92*(1):37–46.
8. Bhutto S, Kaloi A R, Bhutto H. Is Islam Against Science & Technology?. *Indian Journal of ence and Technology*, 2020, *13*(10):1148–1159.
9. Venkatesan A K, Rodriguez B T, Marcotte A R, et al. Using single-particle ICP-MS for monitoring metal-containing particles in tap water. *Environmental ence: Water Research & Technology*, 2018, *4*(12):1923–1932.

10. Davari A R. A Simple Analytical Model to Describe the Impact of Wing on the Flowfield over the Tail in Subsonic Flow. *Aerospaceence & Technology*, 2018, *75*(APR.):88–98.
11. Garcia A R, M.F. Júlio, Ilharco L M. A cork–silica xerogel nanocomposite with unique properties. *Journal of Sol Gel Science & Technology*, 2017, *83*(3):567–573.
12. Penaranda L, Velho L, Sacht L. Real-time correction of panoramic images using hyperbolic Moebius transformations. *Journal of Real Time Image Processing*, 2018, *15*(4):725–738.
13. Manjula G B, Shinde K D. An Innovative Method for Stitching the Images for Panoramic View. *Iosr Journal of Electronics & Communication Engineering*, 2018, *13*(2):44–50.
14. Mizoguchi T. Evaluation of Classification Performance of Pole-Like Objects from MMS Images Using Convolutional Neural Network and Image Super Resolution. *International Journal of Automation Technology*, 2018, *12*(3):369–375.
15. Liao K, Lin C, Zhao Y, et al. OIDC-Net: Omnidirectional Image Distortion Correction via Coarse-to-Fine Region Attention. *IEEE Journal of Selected Topics in Signal Processing*, 2020, *14*(1):222–231.
16. Yan C, Wang Z, Xu C. Gentle Adaboost algorithm based on multi-feature fusion for face detection. *The Journal of Engineering*, 2019, *2019*(15):609–612.
17. Liu J, Hao K, Ding Y, et al. Moving human tracking across multi-camera based on artificial immune random forest and improved colour-texture feature fusion. *Imaging ENCE Journal the*, 2017, *65*(4):1–13.
18. Mantecca P, Kasemets K, Deokar A R, et al. Airborne Nanoparticle Release and Toxicological Risk from Metal-Oxide-Coated Textiles: Toward a Multiscale Safe-by-Design Approach. *Environmental ence and Technology*, 2017, *51*(16):9305–9317.
19. Song W, Wang Y, Shi L, et al. SAR Target Discrimination Algorithm Based on Bag-of-words Model with Multi-feature Fusion. *Journal of Electronics & Information Technology*, 2017, *39*(11):2705–2715.
20. Huanping Z, Yan L, Huojie S. Analysis on Digital Image Re-Ranking Algorithm based on Multi-feature Fusion. *Journal of Engineering ENCE and Technology Review*, 2017, *10*(2):42–50.
21. Howard W, Kiong N S, Jiwei W. Robust Video Tracking Algorithm: A Multi-feature Fusion Approach. *Iet Computer Vision*, 2018, *12*(5):640–650.
22. Sun G, Tang H, Lin K, et al. Automatic Fault Recognition for Key Parts of Train Based on Multi-feature Fusion and BP-AdaBoost Algorithm. *Zhongguo Jixie Gongcheng/China Mechanical Engineering*, 2017, *28*(21):2588–2594.
23. S. Renu, S.H. Krishna Veni. An enhanced CIA tree using string matching algorithm. *International Journal of Applied Engineering Research*, 2017, *12*(16):6123–6126.
24. Puri V, Brancazio D, Harinath E, et al. Demonstration of pharmaceutical tablet coating process by injection molding technology. *International Journal of Pharmaceutics*, 2018, *535*(1–2):106–112.
25. Zhao X, Cheng X, Zhou J, et al. Advanced Topological Map Matching Algorithm Based on D–S Theory. *Arabian Journal for ence & Engineering*, 2017, *43*(5):1–12.
26. Yurong H, Bo W, Zhihong D, et al. Point mass filter based matching algorithm in gravity aided underwater navigation. *Journal of Systems Engineering and Electronics*, 2018, *29*(001):152–159.
27. Shi J, Wang X. A local feature with multiple line descriptors and its speeded-up matching algorithm. *Computer Vision & Image Understanding*, 2017, *162*(SEP.):57–70.
28. Chen C, Ding Y, Xie X, et al. A three-stage online map-matching algorithm by fully using vehicle heading direction. *Journal of Ambient Intelligence & Humanized Computing*, 2018, *9*(5):1–11.
29. Rosa G S, Bergmann J R, Teixeira F L. A Robust Mode-Matching Algorithm for the Analysis of Triaxial Well-Logging Tools in Anisotropic Geophysical Formations. *IEEE Transactions on Geoscience and Remote Sensing*, 2017, *55*(5):2534–2545.
30. Betka A, Terki N, Toumi A, et al. A new block matching algorithm based on stochastic fractal search. *Applied Intelligence*, 2019, *49*(3):1146–1160.